Featured in Physics

Self-similar jet evolution after drop impact on a liquid surface

Cees J. M. van Rijn,[1,*] Jerry Westerweel,[2] Bodjie van Brummen,[2] Arnaud Antkowiak,[3] and Daniel Bonn[1]

[1]*van der Waals-Zeeman Institute, Institute of Physics, University of Amsterdam, Science Park 904, Amsterdam*
[2]*Laboratory for Aero and Hydrodynamics, Delft University of Technology, Mekelweg 2, 2628 CD Delft*
[3]*Institut Jean le Rond d'Alembert, Sorbonne Université, 4 Place Jussieu, 75005 Paris*

(Received 19 June 2020; accepted 22 December 2020; published 5 March 2021)

Small conical-shaped jets may emanate from a liquid bath a short while after a small drop has hit a liquid pool. Here we perform Particle Image Velocimetry (PIV) measurements of the liquid flow inside upward jets after drop impact and show that fluid elements inside the jets may decelerate up to 5–20 times the gravitational acceleration. The measurements show that both the shape of the jet and the velocity profile are self-similar. A theoretical model including surface tension, fluid inertia and gravity correctly predicts the self-similar velocity profile and shape of the jet, allowing us to provide the first quantitative explanation of the shape and dynamics of the emanating jets.

DOI: 10.1103/PhysRevFluids.6.034801

I. INTRODUCTION

Much more than a trillion raindrops hit the earth's surface water every second and a large portion of them generate upward moving jets, typically with a height up to a few centimeter. This happens when such a raindrop hits a pool of water, the drop forms a crater or cavity around the place of impact. When subsequently the water flows back and the cavity collapses, a small water jet is propelled up into the air. These jets have been an object of study by scientists for more than 100 y [1,2] and have also been captured by photographers (Fig. 1) used often in (coffee) commercials, because of their appealing appearance.

That the fluid of the jet substantially comes from a corresponding falling drop is easy to verify: if one lets a drop of milk fall in black coffee from a height of about 5–10 cm; the created jet will be nearly as white as milk. From the moment of droplet impact, the outburst with rise and fall of a jet takes typically less than 100 ms. Numerous studies on this phenomenon have been carried out [3–14], focusing mainly on different fluid responses when a small solid object or a droplet hits the water surface; these include cavity formation, crown splash, central jet rise, and jet tip droplet pinch-off [15–17]. Several theories and fluid simulations [7,13,18] have been developed to relate jet shape to fluid from the bath feeding the jet, however the role of surface tension has remained unclear; only drop formation at the tip has been related to surface tension forces [8,13,14,18,19]. Here we show that capillary forces also determine the shape of the conical jet during its evolution.

Self-similar phenomena have remarkable scale-invariant properties due to the absence of an intrinsic length or timescale. Self-similarity is visible in a wide range of processes such as quasicrystal shape and growth [20,21], stellar collapse [22], fragmentation processes [23], ultrafast asymptotic nonlinear optics [24], single protein dynamics [25], fluid physics [26–28], polymer films [29], complex networks [30,31], and also stochastic processes related to financial markets [31], climatology [32,33], etc. Here we experimentally analyze jet shapes and characterize the inside fluid

*Corresponding author: c.j.m.vanrijn@uva.nl

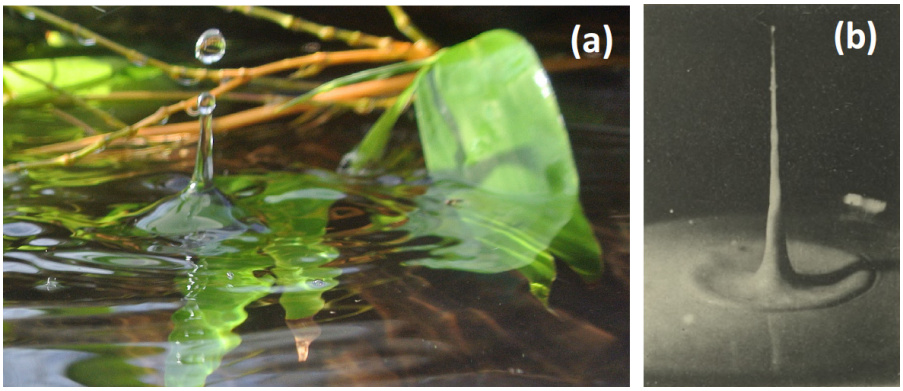

FIG. 1. Jet pictures. (a) After a small (rain)drop has impacted the water surface a jet with accompanying drops at the tip is created. (b) Picture of a milk jet captured by Worthington in 1897 with the aid of instantaneous photography [2].

flow using high-speed particle image velocimetry (PIV), and show that both the velocity profile and the jet shape are self-similar.

II. RESULTS

Figure 2 shows the evolution of a small water jet after impact of a water drop with a diameter of 2.4 mm. A glass tank is filled with water and seeded with the particles. When a droplet falls in the tank, a jet is formed and is illuminated with a continuous wave laser to excite the fluorescent tracer particles (see Supplemental Material (SM), I [18]). By tracking individual fluorescent tracer particles inside the jet it is observed that the particles in the first 10 ms [Fig. 2(d)] decelerate at a much larger rate than can be explained by gravity, typically starting on the order of 50–200 $\mathrm{m/s^2}$ and then leveling off to order 10–20 $\mathrm{m/s^2}$ when the jet approaches maximum height. Possibly surface tension effects can be anticipated to contribute to the strong deceleration of the jet, because in the initial stage of jet formation the ratio of jet surface/jet mass is large.

III. THEORETICAL MODEL

To describe the velocity within the jet, we start from observations of Ghabache *et al.* [4] who argue that the vertical velocity $u(z,t)$ within the jet for non-shock-forming feeding conditions is naturally attracted by a self-similar relaxation wave velocity profile:

$$u(z,t) = \frac{z + z_0}{t + t_0}, \tag{1}$$

where z_0 and t_0 are space and time shifts to match the initial condition. When the tip appears at $t = 0$ and $z = 0$ the tip velocity is given by $u_{\mathrm{tip}} = z_0/t_0$ and remains constant in time. The predicted linear z dependence of Eq. (1) can indeed be observed in Fig. 3(a) and Movies SM2 and SM4, but Fig. 2(d) clearly shows that u_{tip} is not constant in time. Equation (1) is however a simplification and does not account for effects of fluid parameters such as mass density, surface tension, viscosity, or gravity. Taking into account mass density and surface tension solutions for the velocity profile of slender jets have been derived by Ting and Keller [6], who propose a self-similar solution for the jet velocity containing an additional time-dependent term:

$$u(z,t) = \frac{z}{t} - Bt^{1/2}, \tag{2}$$

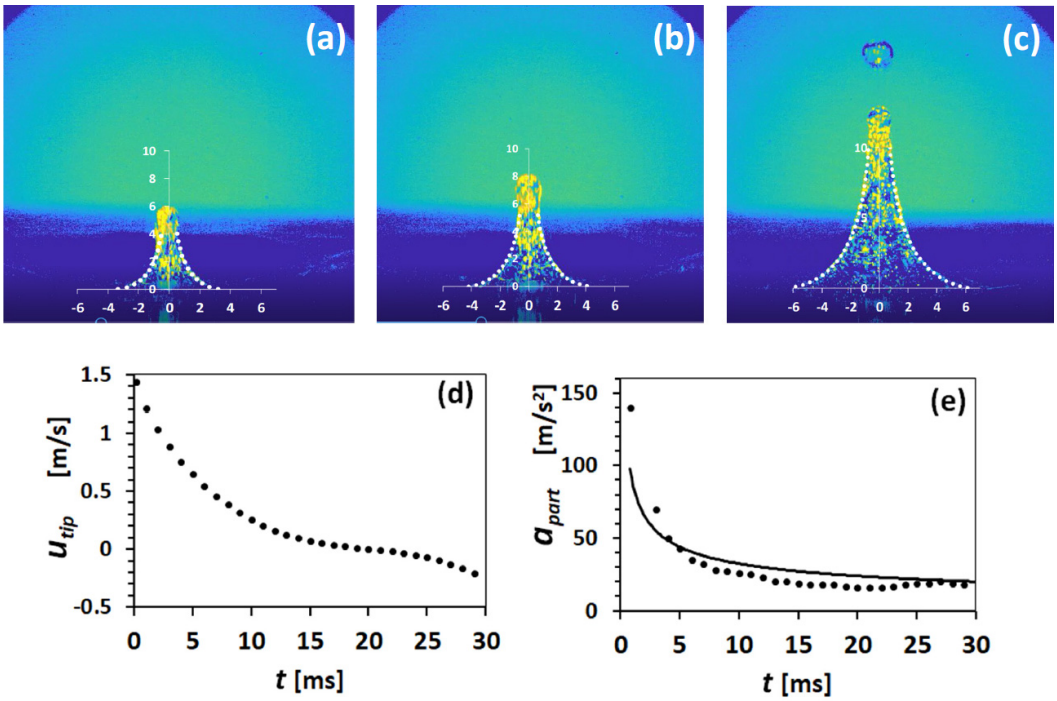

FIG. 2. Evolution of a small water jet containing 15-μm particles (Fluostar). Scale in millimeters. Images taken at a frame rate of 3000 s^{-1} show frames (a)–(c) at 2.64, 10.2, and 17.1 ms after the jet becomes visible at the liquid bath surface (see Supplemental Materials, Movies SM1 and SM2 Jet1 [34]). (d) Velocity plot of the particles in the tip of the jet. (e) Deceleration (i.e., material derivative of the velocity) plot of the particles inside the jet and the tip. Solid line is trendline according to Eq. (4).

with B a positive constant, being proportional to the ratio of surface tension and mass density [6]. This solution was derived by taking into account mass conservation, momentum conservation, and the boundary conditions at the free surface and is valid for jets with a significant surface tension contribution. To verify this, we also experiment with ethanol, having an almost three times lower surface tension than water. In order to account for the contribution of gravity to the velocity profile we use scale-invariance arguments starting from Ting and Keller and derive in dimensional form (see Eq. 23, Supplemental Material II [35]) for the velocity profile:

$$u(z,t) = \frac{z}{t} - Bt^{1/2} - \frac{1}{2}gt. \tag{3}$$

Both the surface tension B term and the gravity term will pull down the jet although with different time exponents.

Calculating the measured particle acceleration $a_{\mathrm{part}}(t)$ inside the jet from the material (convected) derivative of $u(z,t)$: $Du(z,t)/Dt \equiv \partial u/\partial t + u\partial u/\partial z$, the particle deceleration $a_{\mathrm{part}}(t)$ is defined as

$$-\frac{Du(z,t)}{Dt} \equiv a_{\mathrm{part}}(t) = \frac{3\mathrm{B}t^{-(1/2)}}{2} + g. \tag{4}$$

Measured particle deceleration profiles $a_{\mathrm{part}}(t)$ are plotted in Fig. 2(e) and fitted with the solid line to Eq. (4). Please note that particles in the tip of the jet experience the same deceleration as all other particles inside the jet, because Eq. (4) expresses that $a_{\mathrm{part}}(t)$ is uniform (z independent) for all

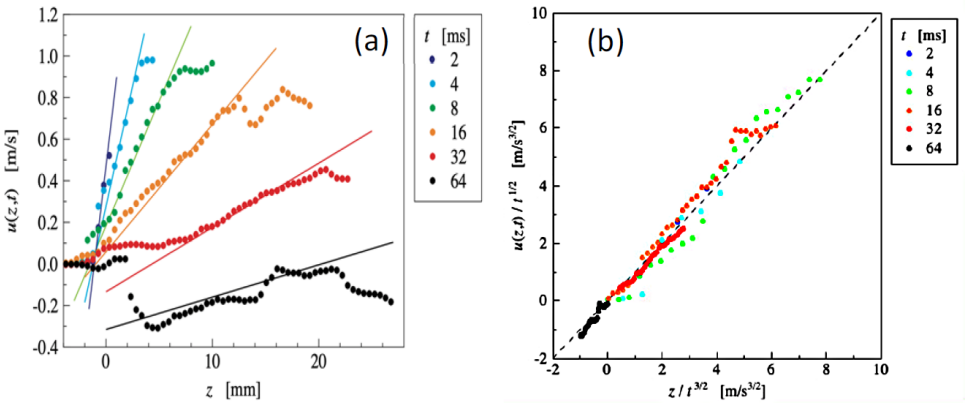

FIG. 3. Velocity plots with respect to the vertical height z for a tall water jet (Supplemental Material, Movies SM3 and SM4 Jet2 [36]) at different times after droplet impact. (a) PIV data at time stamps 2, 4, 8, 16, 32, and 64 ms. (b) Self-similar rescaled velocity profile of the water jet (dotted lines). The gray dashed line is the expected self-similar projection curve of the velocity function Eq. (3), i.e., $u(z,t)/t^{1/2} \approx z/t^{3/2}$–$B$.

particles inside the jet. Experimentally verifying Eqs. (3) and (4) is thus important for the validity of the model.

Substitution of Eq. (4) in (3) yields

$$u(z,t) = \frac{z}{t} - \left[\frac{2}{3}a_{\text{part}}(t) - \frac{1}{6}g\right]t. \tag{5}$$

Since the measured time-dependent values of $a_{\text{part}}(t)$ in the first 20–30 ms are much larger than g [cf. $\frac{2}{3}a_{\text{part}}(t) \gg \frac{1}{6}g$] the direct contribution of gravity in the velocity profile Eq. (5) is rather small. This also implies that in Eq. (3) $\mathrm{B}t^{\frac{1}{2}} \gg \frac{1}{2}gt$. Neglecting in first order the gravity term in Eq. (3) the z dependence of the velocity of the rising jet for different time instants can then be collapsed onto a single straight line by dividing both sides of Eq. (3) by $t^{1/2}$ by plotting $u(z,t)/t^{1/2}$ against $z/t^{3/2}$ [see Fig. 3(b)].

IV. SELF-SIMILARITY

Figure 3(a) shows the velocity profile at time stamps 2, 4, 8, 16, 32, and 64 ms. The solid lines are linear fits to the velocity data showing a decrease of slope in time, that can also be verified by watching Movie SM4. The base levels for $z < 5$ mm of the jets at 32 and 64 ms deviate from the linear fits possibly due to the start of reflow of jet fluid to the bath. In the tip part of the jet the velocity levels off due to drop formation at the tip. The dynamic scaling of the velocity function in Fig. 3(b) shows that the velocity function is self-similar. A dynamic function is said to exhibit dynamic scaling or self-similarity [27] if it satisfies the general condition $f_1(z,t) = t^{\alpha} f_2(\frac{z}{t^{\beta}})$. By choosing $\alpha = 1/2$ and $\beta = 3/2$, the data presented in Fig. 3(b) within error bars correspond to $u(z,t) = t^{\alpha}(\frac{z}{t^{\beta}} - \mathrm{B})$ as indicated by the gray dashed line. The abscissa on the x axis gives $B \approx 1.5 \pm 0.5\,\mathrm{m/s^{3/2}}$. Both axes in Fig. 3(b) are dimensional with unit $\mathrm{m/s^{3/2}}$ but can also be made dimensionless through a division with $L^{-5/4}(\sigma/\rho)^{3/4}$, where L is the chosen unit of length (Supplemental Material II [35]).

We now proceed with the asymptotic jet shape $R(z,t)$. Ghabache *et al.* [4], based on Eq. (1), proposed a general solution in monomial form $R(z,t) \propto z^a t^b$ with $a = -(2b+1)/2$ based on mass conservation only, and argued that a possible solution is $R(z,t) \propto z^{-1}t^{1/2}$. This implies that the dependence of R on parameters z and t reduces to a self-similar function of $z^{-1}t^{1/2}$.

The shape of the jet according to the Ting and Keller [6] model without gravity originates from a balance of the inside pressure $p(z,t)$ of the jet liquid and the capillary pressure $\sigma/R(z,t)$ of the jet

surface. The inside pressure $p(z,t)$ of the jet liquid stems from the inertial forces inside the jet fluid, thus $p(z,t) = a_{\text{part}}(t)\rho z$. This gives $\sigma/R(z,t) = p(z,t) = a_{\text{part}}(t)\rho z$ and an approximate expression for the shape of the jet is then $R(z,t) = \sigma/a_{\text{part}}(t)\rho z$. The full self-similar expression for $R(z,t)$ obtained by Ting and Keller [6] is

$$R(z,t) = \frac{\sigma}{3\rho \mathrm{B} t}\left(\frac{z}{2t^{3/2}} + B\right)^{-1} = \frac{\sigma}{\rho a_{\text{part}}(t)\left[z + \frac{4}{3}a_{\text{part}}(t)t^2\right]}. \tag{6}$$

In order to account for the contribution of gravity to the jet shape we use similar scale-invariance arguments starting from Ting and Keller (6) and find in dimensional form (Eq. (23), Supplemental Material II [35]) for the shape of the jet:

$$R(z,t) = \frac{\sigma}{3\rho \mathrm{B} t}\left(\frac{z}{2t^{\frac{3}{2}}} + \mathrm{B} + \frac{1}{4}g\sqrt{t}\right)^{-1} = \frac{\sigma}{\rho\left[a_{\text{part}}(t) - g\right)\left(z + \frac{4}{3}(a_{\text{part}}(t) - \frac{5g}{8})t^2\right]}. \tag{7}$$

The main difference between Eqs. (6) and (7) is the division by the term $a_{\text{part}}(t) - g$ instead of $a_{\text{part}}(t)$. By taking into account gravity, the inside pressure $p(z,t)$ of the jet liquid is now the sum of the inertial pressure from the inertial forces (including gravity) inside the jet fluid and of the hydrostatic pressure, i.e., $p(z,t) = [a_{\text{part}}(t) - g]\rho z$ and not $p(z,t) = a_{\text{part}}(t)$ in the case without gravity. In the initial stage of the jet when $a_{\text{part}}(t) \gg g$ gravity will hardly influence the jet shape. Because the particle acceleration $a_{\text{part}}(t) \equiv (3/2)Bt^{-1/2} + g$ [Eq. (4)] has a term decreasing with a square-root dependence in time, then in a later stage, typically after 2050 ms, we reach a regime in that $a_{\text{part}}(t) \approx g$. Then the total internal pressure $p(z,t) = [a_{\text{part}}(t) - g]\rho z$ becomes almost zero over the entire height of the jet, and the jet may lose its concave shape according to Eq. (7).

During the evolution of the jet the water level from which the jet forms is always deeper than the surface level of the bath, typically $\approx$ 1–2 mm or less. In Eq. (7) we see that $R(z,t)$ becomes infinite when $z(t) = -\frac{4}{3}[a_{\text{part}}(t) - \frac{5}{8}g]t^2$. This term is also typically $\approx$ 1–2 mm in the first 20–30 ms of the jet formation. So, if we define $z_0(t) = \frac{4}{3}[a_{\text{part}}(t) - \frac{5}{8}g]t^2$ we have a measure to estimate deviations of the actual base surface level of the jet at $z \approx z_0(t)$ with respect to the surface level of the liquid bath, where the hydrostatic pressure is zero.

V. DISCUSSION

The Ting and Keller slender jet solution Eq. (6) without the contribution from gravity [orange dashed line in Fig. 4(a)] does not give a good value for the jet width using the experimental determined particle deceleration $a_{\text{part}} = 2.6\,\text{m/s}^2$ at $t = 27$ ms in Eq. (6). Including the contribution from gravity using Eq. (7) gives a much better fit of the actual experimental width [white dotted line in Fig. 4(a)] as well as of the jet shape. The green dashed line in Fig. 4(a) is a best fit of only the jet shape according to the simple equation $R(z,t) \propto z^{-1}$, which shows a significant deviation from the actual contour.

In Fig. 4(b) we demonstrate the self-similarity in both the time and space domain by replotting the actual jet contour where the coordinates have been made dimensionless by dividing them by $\sqrt{\sigma/\rho[a_{\text{part}}(t) - g]}$. The figure shows that the evolution of the jet shape occurs self-similar by choosing the general self-similar condition $R(z,t) = t^{\alpha}\phi(\frac{z}{t^{\beta}})$ with coefficients $\beta = 0$, and $\alpha = -1/2$.

The physical parameters that determine both jet dynamics and shape according to the model are surface tension, mass density, gravity and time dependent particle acceleration as given by Eqs. (5)–(7). In particular the shape of the jet is primarily determined by the ratio of surface tension and mass density Eq. (7) and corrected for gravity. We varied both the surface tension the density by choosing ethanol ($\sigma = 22.1$ mN/m, $\rho = 0.789$ g/cm^3) and pure water ($\sigma = 72.0$ mN/m, $\rho = 0.998$ g/cm^3) experiments, the corresponding surface tension mass density ratio varies thus about 250%. The results from experiments using ethanol (Fig. 2 Supplemental Material III [37]) are in agreement with Eq. (7), demonstrating the robustness of our findings. In order to check a possible contribution of viscosity we have performed and analyzed additional water/glycerol PIV

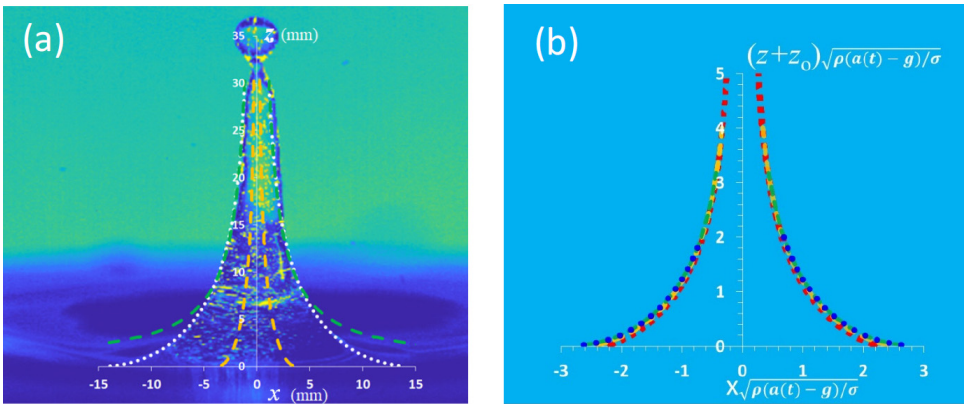

FIG. 4. Snapshots and model plots of self-similar jet shapes of a tall water jet (Movies SM3 and SM4 Jet2). (a) Picture at 27 ms after initial outburst of the jet with three fits to the jet; (1) a best fit of only the jet shape (green dashed line) according to $R(z,t) \propto z^{-1}t^{1/2}$ as proposed by Ghabache *et al.* [4]; (2) an actual experimental width fit according to the Ting and Keller slender jet model Eq. (6) without taking into account the contribution from gravity (orange dashed lines); and (3) the gravity-corrected model Eq. (7) with a shape and actual experimental width fit (white dotted lines). (b), Self-similar dimensionless jet shapes as derived from Eq. (7) for the water jet Movie SM3 and for the ethanol jet of Fig. 2, Supplemental Material, III [37]. The jet shape plots for water are at time $t = 4$ ms (blue dots), 8 ms (green dashes), 16 ms (orange dashes), and for ethanol at 20 ms (red squares).

experiments (Supplemental Material IV [38] with different viscosities up to 10 mPas, and observe a jet shape and width of the jet according to Eq. (7). It would be interesting to study the formation and evolution of the jet in the absence of gravity; the fluid flow dynamics inside the formed cavity will drastically change due to the absence of gravity and buoyancy; so the initial jet eruption stage will change, and in the late stage of the jet, due to the absence of a hydrostatic pressure, the shape of the jet will be more and longer determined by the capillary pressure contribution.

VI. CONCLUSION

In summary, we found that upward jets resulting from drop impact on a fluid surface evolve with a similar shape and self-similar velocity profile, corresponding to one particular solution in Ting and Keller's [6] family of self-similar solutions, which solution has now been corrected for the contribution from gravity. That only one particular self-similar solution is preferred out of a whole family of solutions is reminiscent of the viscous fingering or Saffman-Taylor instability [39], for which the surface tension is a singular perturbation that selects the finger shape from a family of permitted shapes.

[1] A. M. Worthington, On impact with a liquid surface, Proc. R. Soc. London **34**, 217 (1882).
[2] A. M. Worthington and R. S. Cole, Impact with a liquid surface studied by the aid of instantaneous photography, Phil. Trans. R. Soc. Ser. A **189**, 137 (1897).
[3] A. M. Gañán-Calvo, Scaling laws of top jet drop size and speed from bubble bursting including gravity and inviscid limit, Phys. Rev. Fluids **3**, 091601(R) (2018).
[4] E. Ghabache, T. Séon, and A. Antkowiak, Liquid jet eruption from hollow relaxation, J. Fluid Mech. **761**, 206 (2014).
[5] C. J. M. van Rijn, Emanating jets as shaped by surface tension forces, Langmuir **34**, 13837 (2018).

[6] L. Ting and J. B. Keller, Slender jets and thin sheets with surface tension, SIAM J. Appl. Math. **50**, 1533 (1990).
[7] B. W. Zeff, B. Kleber, J. Fineberg, and D. P. Lathrop, Singularity dynamics in curvature collapse and jet eruption on a fluid surface, Nature (London) **403**, 401 (2000).
[8] A. S. Ismail, A. M. Gañán-Calvo, J. R. Castrejón-Pita, M. A. Herrada, and A. A. Castrejón-Pita, Controlled cavity collapse: Scaling laws of drop formation, Soft Matter **14**, 7671 (2018).
[9] M. Rein, The transitional regime between coalescing and splashing drops, J. Fluid Mech. **306**, 145 (1996).
[10] J. Eggers, M. A. Fontelos, D. Leppinen, and J. H. Snoeijer, Theory of the Collapsing Axisymmetric Cavity, Phys. Rev. Lett. **98**, 094502 (2007).
[11] H. Zhao, A. Brunsvold, and S. T. Munkejord, Investigation of droplets impinging on a deep pool: Transition from coalescence to jetting, Exp. Fluids **50**, 621 (2011).
[12] S. L. Manzello and J. C. Yang, An experimental study of a water droplet impinging on a liquid surface, Exp. Fluids **32**, 580 (2002).
[13] S. Gekle, J. M. Gordillo, D. van der Meer, and D. Lohse, High-Speed Jet Formation after Solid Object Impact, Phys. Rev. Lett. **102**, 034502 (2009).
[14] J. O. Marston and S. T. Thoroddsen, Apex jet from impacting drops, J. Fluid Mech. **614**, 293 (2008).
[15] A. L. Yarin, Drop impact dynamics: Splashing, spreading, receding, bouncing, Ann. Rev. Fluid Mech. **38**, 159 (2006).
[16] X. D. Shi, M. P. Brenner, and S. R. Nagel, A cascade of structure in a drop falling from a faucet, Science **265**, 219 (1994).
[17] J. Eggers and T. F. Dupont, Drop formation in a one-dimensional approximation of the Navier–Stokes equation, J. Fluid Mech. **262**, 205 (1994).
[18] See Supplemental Material at http://link.aps.org/supplemental/10.1103/PhysRevFluids.6.034801 for the experimental setup.
[19] E. Castillo-Orozco, A. Davanlou, P. K. Choudhury, and R. Kumar, Droplet impact on deep liquid pools: Rayleigh jet to formation of secondary droplets, Phys. Rev. E. **92**, 053022 (2015).
[20] K. Kamiya, T. Takeuchi, N. Kabeya, N. Wada, T. Ishimasa, A. Ochiai, K. Deguchi, K. Imura, and N. K. Sato, Discovery of superconductivity in quasicrystals, Nat. Commun. **9**, 154 (2018).
[21] A. E. Madison, Self-similarity and self-inversion of quasicrystals, Phys. Solid State **56**, 1706 (2014).
[22] A. Yahil, Self-similar stellar collapse, Astrophys. J. **265**, 1047 (1991).
[23] J. Bertoin, On small masses in self-similar fragmentations, Stoch. Process. Appl. **109**, 13 (2004).
[24] A. Nazarkin, A. Abdolvand, A. V. Chugreev, and P. St.J. Russell, Direct Observation of Self-Similarity in Evolution of Transient Stimulated Raman Scattering in Gas-Filled Photonic Crystal Fibers, Phys. Rev. Lett. **105**, 173902 (2010).
[25] X. Hu, L. Hong, M. D. Smith, T. Neusius, X. Cheng, and J. C. Smith, The dynamics of single protein molecules is non-equilibrium and self-similar over thirteen decades in time, Nat. Phys. **12**, 171 (2016).
[26] M. C. Dallaston, M. A. Fontelos, D. Tseluiko, and S. Kalliadasis, Discrete Self-Similarity in Interfacial Hydrodynamics and the Formation of Iterated Structures, Phys. Rev. Lett. **120**, 034505 (2018).
[27] J. Eggers and M. Fontelos, Similarity profile, in *Singularities: Formation, Structure, and Propagation*, (Cambridge University Press, Cambridge, 2015), pp. 32–62.
[28] A. Lagarde, C. Josserand, and S. Protrière, Oscillating path between self-similarities in liquid pinch-off, Proc. Natl. Acad. Sci. USA **115**, 12371 (2018).
[29] J. D. McGraw, T. Salez, O. Bäumchen, E. Raphaël, and K. Dalnoki-Veress, Self-Similarity and Energy Dissipation in Stepped Polymer Films, Phys. Rev. Lett. **109**, 128303 (2012).
[30] C. Song, S. Havlin, and H. A. Makse, Self-similarity of complex networks, Nature (London) **433**, 392 (2005).
[31] M. Ángeles Serrano, D. Krioukov, and M Boguñá, Self-Similarity of Complex Networks and Hidden Metric Spaces, Phys. Rev. Lett. **100**, 078701 (2008).
[32] M. Menabde, Self-similar random fields and rainfall simulation, J. Geophys. Res.: Atmos. **102**, 13509 (1997).
[33] F. Simini, T. Anfodillo, M. Carrer, J. R. Banavar, and A. Maritan, Self-similarity and scaling in forest communities, Proc. Natl. Acad. Sci. USA **107**, 7658 (2010).

[34] See Supplemental Material at http://link.aps.org/supplemental/10.1103/PhysRevFluids.6.034801 for the movies SM1 and SM2.
[35] See Supplemental Material at http://link.aps.org/supplemental/10.1103/PhysRevFluids.6.034801 for the note on gravity.
[36] See Supplemental Material at http://link.aps.org/supplemental/10.1103/PhysRevFluids.6.034801 for the movies SM1 and SM2.
[37] See Supplemental Material at http://link.aps.org/supplemental/10.1103/PhysRevFluids.6.034801 for the results with ethanol.
[38] See Supplemental Material at http://link.aps.org/supplemental/10.1103/PhysRevFluids.6.034801 for the results with water/glycerol.
[39] P. G. Saffman and G. Taylor, The penetration of a fluid into a medium or Hele-Shaw Cell containing a more viscous liquid, Proc. Royal Soc. London, Ser. A **245**, 312 (1958).